

Performance of an electron gun for a high-brightness X-ray generator

Takashi Sugimura,* Satoshi Ohsawa and Mitsuo Ikeda

Received 31 July 2007

Accepted 13 December 2007

Accelerator Laboratory, High Energy Accelerator Research Organization (KEK), Japan.

E-mail: takashi.sugimura@kek.jp

A prototype thermionic electron gun for a high-brightness X-ray generator has been developed. Its extraction voltage and design current are 60 kV and 100 mA (DC), respectively. The X-ray generator aims towards a maximum brilliance of 60 kW mm^{-2} . The beam sizes at the rotating anticathode must therefore be within $1.0 \text{ mm} \times 0.1 \text{ mm}$ and a small beam emittance is required. The fabricated electron gun optimizes an aperture grid and a Whenelt electrode. The performance of the prototype electron gun measured using pulsed-beam tests is as follows: maximum beam current, 85.7 mA; beam focus size at the rotating anticathode, $0.79 \text{ mm} \times 0.13 \text{ mm}$. In DC beam tests, FWHM beam sizes were measured to be $0.65 \text{ mm} \times 0.08 \text{ mm}$ at the rotating anticathode with a beam current of 45 mA. The beam current recently reached $\sim 60 \text{ mA}$ with some thermal problems.

© 2008 International Union of Crystallography
Printed in Singapore – all rights reserved

Keywords: electron gun; DC beam; X-ray generator.

1. Introduction

We have been developing a thermionic electron gun with an aperture grid for a high-brightness X-ray generator (Ohsawa *et al.*, 2005; Sugimura *et al.*, 2006, 2007). The X-ray generator is equipped with a newly designed rotating anticathode proposed by Sakabe *et al.* (2007) and aims towards a maximum brilliance of 60 kW mm^{-2} . In order to increase the brilliance, an increase in the electron beam power and a decrease in beam size are required. Generally, a higher beam current causes a larger beam emittance, and a larger beam emittance brings a larger beam size. Thus optimization of the electron gun design is important. Since some design parameters of the electron gun, such as extraction voltage, grid voltage and maximum beam current, are restricted by existing high-voltage power supplies, it is the shape of the electrodes that is mainly optimized. Owing to emittance growth at the grid electrode and damage of grid electrodes caused by its own beam, we introduced an aperture grid electrode instead of a conventional mesh grid. Optimization of the shape of the electrodes are based on EGUN (Herrmansfeldt, 1988) simulation results, which predicted that the extracted current will reach 145 mA and normalized emittance will be $3\pi \text{ mm mrad}$ for the optimized electron gun. These values meet the required performance. Table 1 summarizes the main specifications of the electron gun.

The first prototype electron gun with the optimized electrode was fabricated and proffered for beam tests. Fig. 1 shows the cathode-grid assembly. In order to avoid destroying the electron gun by its own beam, initial beam tests were performed with a pulsed beam. In the first stage of the pulsed beam tests, the extracted beam current at a fixed target was measured as a function of grid voltage with fixed anode voltage and transport system which is almost identical to the real prototype. A maximum beam current of 85.7 mA was obtained at a grid voltage of 2.8 kV. Although this value is slightly less than the specification value, we did not apply a higher voltage to the grid on

Table 1

Main specifications of the electron gun.

Component	Specifications
Extraction voltage	60 kV
Maximum current	> 100 mA
Grid type	Aperture grid
Cathode emission	Thermionic
Cathode material	LaB ₆ or CeB ₆
Cathode diameter	2.0 mm
Cathode-grid voltage	5.0 kV (DC)/3.5 kV (pulse)
Beam size at anticathode	< 1.0 mm × 0.1 mm
Normalized emittance	A few $\pi \text{ mm mrad}$

account of the high frequency of discharge which comes from a lack of the aging process.

2. Beam tests as an X-ray generator

2.1. Pulsed beam tests

The electron gun was installed in the X-ray generator in order to measure the beam sizes at the rotating anticathode. Owing to space limitations, the extraction voltage, grid-pulse voltage and heater power were supplied from a distance by power supplies through 25 m-long high-voltage cables. In particular, the grid-pulse voltage was transmitted by triaxial cable. In order to match impedance between the cable and the electron gun, a hand-wound transformer was inserted. The transformer enables the output voltage of the grid pulsar to be lowered to about one-fifth of that without the transformer. Since stored energy in the triaxial cable is supplied to the electron gun, the discharge became more violent. Complete grounding of the floating conductive materials and careful aging process suppressed the discharge.

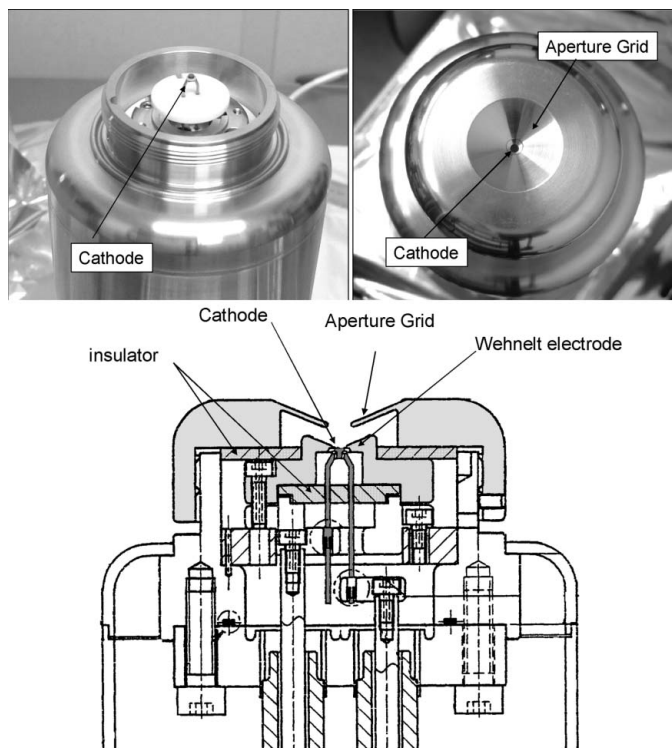


Figure 1 Images of the cathode-grid assembly and a cross-sectional view. The cathode, of diameter 2 mm, is located on the white ceramic insulator (left). The aperture grid is threaded into the top of a stem (right). The sectional drawing of the cathode-grid assembly shows the detailed structure of the electron gun (bottom).

After optimization of the optics caused by small modifications of the transport system alignments, a beam current of 80 mA was achieved at the grid-pulse voltage which was equivalent to a grid voltage of 1.2 kV. An X-ray image on a fluorescent screen, enlarged several times using a pinhole of diameter 10 μm , was recorded using a cooled CCD camera. Fig. 2 shows a schematic layout of the X-ray measurement system. From an analysis of the recorded data, FWHM sizes of the beam at the anticathode were observed to be 0.79 mm

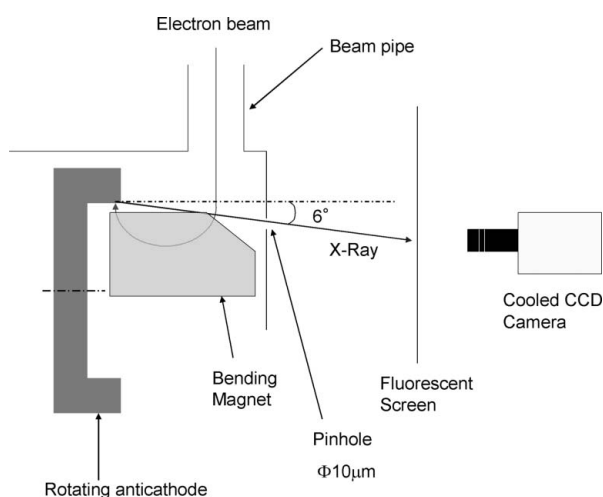


Figure 2 Schematic view of the X-ray measurement system. X-rays from the anticathode are projected through a pinhole to a fluorescent screen, which is positioned at an angle of 6° against the anticathode surface. Visible light from the fluorescent screen is recorded by a cooled CCD camera.

(horizontal) and 0.13 mm (vertical). These values almost satisfy the specification values.

2.2. DC beam tests

2.2.1. DC beam test 1. Since DC beam tests risk melting the vacuum chamber with a well focused beam with a current of only a few mA, the beam must be carefully controlled. In the first stage of the DC beam tests the beam current was limited by remote-controlled grid voltage and the heater current was fixed at 2.6 A, which was large enough for the beam current. Since the maximum output current of the DC high-voltage power supply used in the pulsed beam tests was insufficient for DC beam tests, it was replaced by another DC high-voltage power supply whose maximum voltage and current were 60 kV and 100 mA, respectively. Fig. 3 shows a schematic configuration of the DC beam tests.

This power supply oscillates when it operates at a low current below ~10 mA. Its voltage variation extends over $\pm 10\%$ of output voltage. Fig. 4 shows the wave form of the output voltage. The measured frequency of the vibration is 4.7 Hz. We introduced a combined resistance of 4.8 M Ω parallel to the electron gun in order to reduce the oscillation phenomena. This will limit the maximum beam current below 87.5 mA from the perspective of power consumption.

We stepped up the grid voltage from -400 V to 0 V and obtained a beam current of 6 mA. Fig. 5 shows the beam profile on the anticathode. The approximate beam size of 0.23 mm \times 1.3 mm is larger than that of the pulsed beam.

The peripheries of a beam pipe which connect the chambers for the electron gun and the rotating anticathode gave out a foul smell and had a high temperature. Although we put thermocouple sensors on

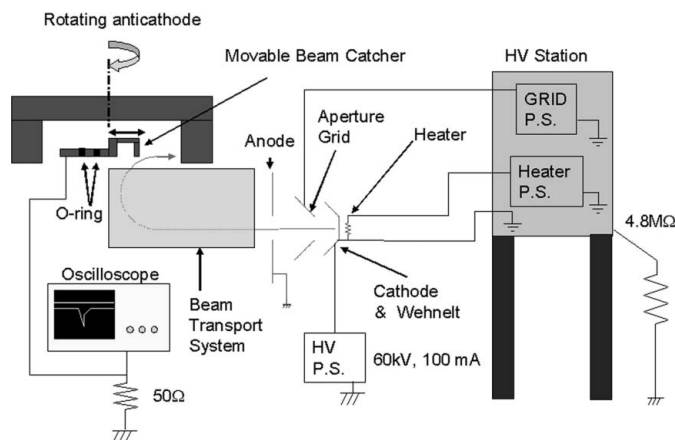


Figure 3 System configuration for DC beam tests.

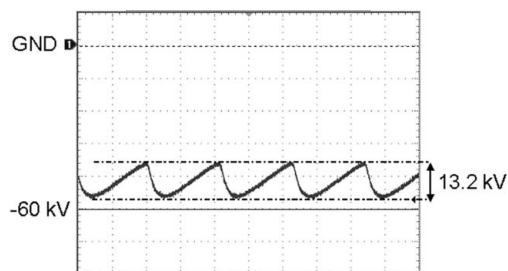


Figure 4 Voltage vibration of the high-voltage power supply without load.

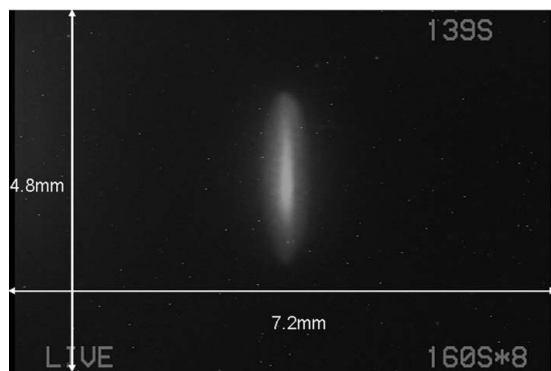


Figure 5 Beam profile on the anticathode without grid voltage. The approximate beam size is $0.23 \text{ mm} \times 1.3 \text{ mm}$. It is larger than that of the pulsed beam.

the beam pipe and adjusted the beam optics in order to lower the temperature, it was 321 K with a beam current of 6 mA. Measured beam sizes at the target were still larger.

2.2.2. Countermeasures. The beam pipe of 6 mm inner diameter was rather narrow for the simulated beam size of 3.5 mm. Thus the beam pipe was drilled to have an inner diameter of 10.0 mm and a length of 10.5 cm. Naturally cooling electromagnets, narrowly girdled around the beam pipe, were upgraded to air-cooling ones using a blower.

The start-up sequence was also changed. In pulsed beam tests, we set the heater current and the extraction voltage to fixed values followed by stepping up the grid voltage in order to control the beam current. Since the electron gun has been optimized for an operating grid voltage of 3 kV, operation around the grid voltage of 0 V is beyond the scope of the assumption.

Fig. 6 shows a comparison of the beam trajectories simulated using the EGUN code. Fig. 6(a) shows the result for a grid voltage of 3.0 kV and Fig. 6(b) shows that for 1 V. The trajectory is spread out after the narrow part in Fig. 6(b), while it is almost parallel in Fig. 6(a). As for the beam current, it is becoming obviously lower from 145 mA in case (a) to 5.9 mA in case (b). This value is limited by space charge and is almost the same as the obtained beam current of 6 mA. The newly refined start-up sequence is as follows: (i) set the grid voltage to 3.0 kV; (ii) set the extraction voltage to 60 kV; (iii) step up the heater current so as to obtain the required beam current. Although we were afraid that a space-charge effect difference owing to the heater-limited beam current might have some effect on the beam in the new sequence, it turned out to be negligibly small in the following beam tests.

2.2.3. DC beam tests 2. After taking the above countermeasures into account, serious increases in temperature at the beam pipe did not occur with a beam current of 6 mA. FWHM beam sizes obtained by fitting to a Gaussian curve with a beam current of 27 mA are $0.77 \text{ mm} \times 0.11 \text{ mm}$ at the anticathode. These values are almost the same as those of the pulsed beam.

Another thermal problem occurred at the vacuum chamber near the anticathode. Although the chamber had been forced-air-cooled by an air compressor, the temperature of the chamber was almost 373 K. We also found that a small part of the beam hit the movable beam catcher located near the anticathode for measuring the beam current. The beam current captured by the beam catcher stepped aside from the main part of the beam was 0.4 mA. Although the input power which corresponds to 24 W is not too large, the beam catcher, which is isolated and has a small thermal heat capacity, easily reaches a high temperature. We suspected damage to the O-rings used as the

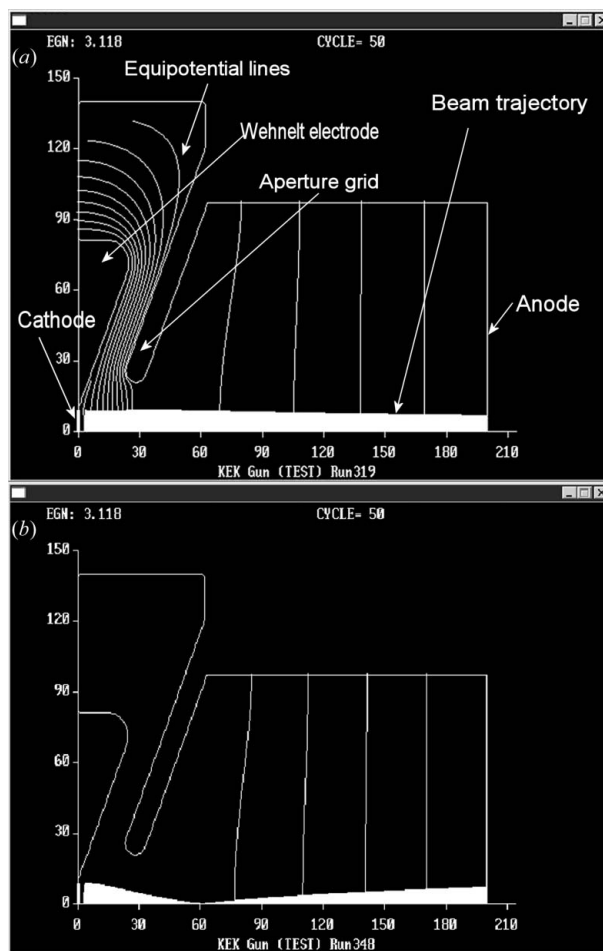


Figure 6 Beam trajectories calculated using EGUN simulations. (a) The beam is extracted almost parallel, with a grid voltage of 3 kV. (b) The beam is spread out after the waist of the beam, with a grid voltage of 1 V.

vacuum interface of the beam catcher, shown in Fig. 3. Fig. 7 shows a photograph of the vacuum chamber and the beam catcher. The beam catcher is located in the slot of the chamber, and the surface of the chamber near the beam catcher is tarnished. Fig. 8 shows a photograph of the anticathode. The anticathode made of copper is also tarnished except for the central part of it. These tarnishings are due to chemical vapour deposition of silicon derived from the silicon grease applied to the O-rings. Tarnishing may induce an insulator breakdown or decrement of transparency of the windows for optical observations. A distance of 0.5 mm between the beam catcher and the center of the beam orbit had been too small. We prepared a new beam catcher which could maintain a distance of 3.1 mm from the center of the beam orbit. Although the beam current captured by the new beam catcher when it stepped aside from the main part of the beam has been reduced to about one-sixth, it is not sufficient. The distance of 3.1 mm is still too small. The beam catcher will be removed at the next vacuum purge.

We added water-cooling tubes on the vacuum chamber near the anticathode and increased the power of the air compressor to 2.2 kW. These cooling systems reduced the temperature of the vacuum chamber by about 40 K. We have been increasing the beam current with care in terms of the temperature and vacuum pressure towards the goal current. Fig. 9 shows the beam profile at a beam current of 45 mA. Obtained FWHM beam sizes from the profile are $0.65 \text{ mm} \times$

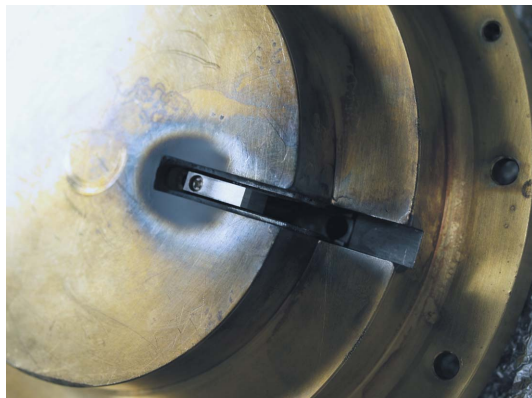


Figure 7
Inner surface of the vacuum chamber. The beam catcher is seen in the slot of the chamber. The surface of the chamber near the beam catcher is tarnished.

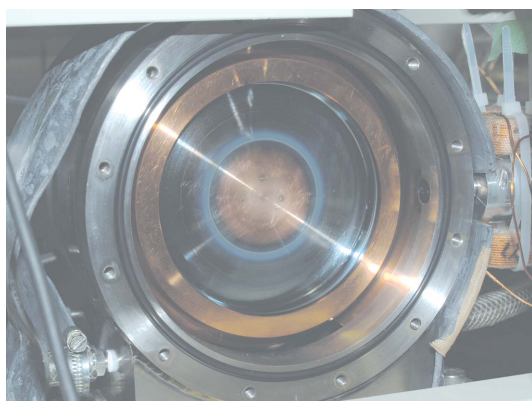


Figure 8
The anticathode in the vacuum chamber. The anticathode made of copper is tarnished except for its center.

0.08 mm. Effective brilliance, which is defined here to be the average density of the beam power within an ellipse whose major and minor axes lengths are equal to the FWHM beam sizes, is 34 kW mm^{-2} under the assumption that the beam on the target has a two-dimensional Gaussian profile. Taking the total current of 45 mA into consideration, this value is mildly impressive. An increase in the beam current will deliver the expected brilliance. Recently a beam current of approximately 60 mA was achieved.

3. Summary

A prototype thermionic electron gun with an aperture grid for a high-brightness X-ray generator has been developed. In the DC beam tests



Figure 9
DC beam profiles on the anticathode. FWHM beam sizes are $0.65 \text{ mm} \times 0.08 \text{ mm}$ with a beam current of 45 mA.

performed after the pulsed beam tests the FWHM beam sizes are measured to be $0.65 \text{ mm} \times 0.08 \text{ mm}$ at the anticathode with a beam current of 45 mA. This corresponds to an effective brilliance of 34 kW mm^{-2} . Although the problem to be solved in the DC beam tests has been a thermal one, a beam current of approximately 60 mA has recently been achieved with an extraction voltage of 60 kV. The beam current will increase, taking care with the heating, and the target brilliance of 60 kW mm^{-2} will be accomplished in the not so distant future.

The work presented here is a collaborative project with the Foundation for Advancement of International Science (FAIS). The authors would like to give their sincere thanks to Professor Noriyoshi Sakabe for his close cooperation.

References

- Herrmansfeldt, W. B. (1988). SLAC Report 331. SLAC, CA, USA.
- Ohsawa, S., Ikeda, M., Sugimura, T., Tawada, M., Hozumi, Y. & Kanno, K. (2005). *Proceedings of the 2005 Particle Accelerator Conference (PAC2005)*, Knoxville, TN, USA, pp. 1488–1490.
- Sakabe, N., Ohsawa, S., Sugimura, T., Ikeda, M., Tawada, M., Watanabe, N., Sasaki, K., Ohshima, K., Wakatsuki, M. & Sakabe, K. (2007). *2nd International Symposium of Diffraction Structural Biology 2007*, Tokyo, Japan.
- Sugimura, T., Ohsawa, S. & Ikeda, M. (2007). *Proceedings of the 2007 Particle Accelerator Conference (PAC2007)*, Albuquerque, NM, USA, pp. 2775–2777.
- Sugimura, T., Ohsawa, S., Ikeda, M., Hozumi, Y. & Kanno, K. (2006). *Proceedings of the 3rd Annual Meeting of the Particle Accelerator Society of Japan and the 31st Linear Accelerator Meeting in Japan*, 2–4 August 2006, Sendai, Japan, pp. 532–535. (In Japanese.)